CYBERNETICS AND PHYSICS, VOL. 15, NO. 1, 2026, 64–70

Right-Ventricular Myocardial Perfusion Gated SPECT Data Processing Using a Deep Learning Model

Petr Larochkin
St. Petersburg State University
Russia
plarochkin@gmail.com

Elena Kotina
St. Petersburg State University
Russia
e.kotina@spbu.ru

Article history:
Received 18.04.2026, Accepted 19.06.2026

Abstract

A sequence-based deep learning pipeline is proposed for automated processing of gated SPECT studies of the right ventricle. The model processes a temporal sequence of 3D tomographic volumes and predicts right-ventricular myocardial masks for each cardiac phase. Based on the predicted segmentation masks, clinical parameters are computed and perfusion polar maps of the "bull's eye" type, as well as magnitude and phase planar maps, are constructed. In experiments, the recurrent model achieved a Dice score of up to 0.8119.

Key words

Gated single photon emission computed tomography (gSPECT), myocardial perfusion imaging, deep learning, image segmentation, functional images

1 Introduction

Myocardial perfusion imaging with single photon emission computed tomography (SPECT) is a nuclear medicine modality that relies on cardiotropic radiopharmaceuticals and gamma cameras. SPECT systems record gamma photons emitted by radioisotopes within the tracer. The radiopharmaceuticals used in this study are distributed in the myocardium approximately proportionally to blood flow [Ostroumov et al., 2010; Ryzhkova, 2016]. Nuclear cardiology provides clinically important diagnostic and prognostic information that is not fully captured by other modalities such as magnetic resonance imaging (MRI), computed tomography (CT) or echocardiography [Ostroumov et al., 2010].

In standard clinical workflows, the processing of gated SPECT (gSPECT) studies produces not only an evaluation of coronary microcirculation, but also functional parameters of the left ventricle (LV), including end-diastolic and end-systolic volumes, ejection fraction, indices of regional motion abnormalities and systolic wall thickening [Ostroumov et al., 2010; Ploskikh and Kotina, 2018; Ploskikh and Kotina, 2021].

The most widely used software packages focus on LV analysis. The right ventricle (RV) is commonly not processed due to its highly variable anatomy and relatively low tracer uptake. However, when the RV is visible, assessment of RV perfusion and function can provide additional diagnostic and prognostic information in cardiovascular disease [Jose et al., 2022; Brunken, 2022; Mannting et al., 1999; Meyer et al., 2010; Farag et al., 2019]. Consequently, RV analysis has been an active area of research and has been addressed in multiple studies [Jose et al., 2022; Brunken, 2022; Mannting et al., 1999; Meyer et al., 2010; Farag et al., 2019; Entezarmahdi et al., 2023; Kotina et al., 2014; Rich and Ward, 2010].

With the advancement of neural networks, deep learning has become a practical approach to medical image segmentation [Schmidt et al., 2023; Larochkin et al., 2025]. In this work, a recurrent deep learning model is used for automatic segmentation of the right ventricle in myocardial perfusion gSPECT. A gated study provides a sequence of tomographic volumes corresponding to different phases of a "representative cardiac cycle" [Ostroumov et al., 2010; Ploskikh and Kotina, 2018]. The previous approach focused on segmenting a single 3D volume [Larochkin et al., 2025]. Here, a model is used that takes the entire study as input, i.e. a sequence of N 3D volumes, allowing temporally consistent segmentation and explicit use of the time component.

Most existing algorithms are primarily designed for LV analysis, whereas methods for RV processing

Setting	Value
Backbone	ResUNetSE3D + ConvLSTM
Channels	[16, 64, 128, 256]
Optimizer	AdamW, lr= 10^{-4}
Loss	BCEDiceBoundaryLoss
Batch size	2

Table 1. Architecture and training hyperparameters of the RecurrentUNet3D segmentation model

are less extensively developed. Previous work includes semi-automatic approaches [Kotina et al., 2014] to RV myocardial segmentation without neural networks and methods tailored to non-gated studies [Farag et al., 2019; Entezarmahdi et al., 2023].

The resulting segmentation enables computation of clinically relevant parameters and construction of functional images.

2 Problem statement

Automated quantitative assessment of right-ventricular perfusion and function from gSPECT requires solving several coupled subproblems: constructing consistent 3D myocardial masks and calculating diagnostic characteristics from these masks. In previous work [Larochkin et al., 2025], the segmentation model processed a single 3D tomographic volume. In this work, the model processes sequences of volumes, and clinical and diagnostic parameters are computed from the masks.

Accordingly, the following interconnected tasks for analyzing gated right-ventricular SPECT studies are considered:

1. 3D segmentation of the right-ventricular myocardium. Binary 3D masks of the RV myocardium are automatically predicted for each cardiac phase.
2. Computation of clinical parameters. After segmentation, the RV cavity is extracted and a time-dependent volume curve is formed. From the temporal dynamics of volume, end-diastolic and end-systolic volumes and additional rate-based indices are computed.
3. Polar map construction. RV myocardial perfusion polar maps are constructed in the standard "bull's eye" planar representation [Ploskikh and Kotina, 2018] that supports quantitative regional perfusion assessment. Phase and magnitude planar maps are computed from the set of polar maps of perfusion across all cardiac phases.

Two input data configurations are considered for the same recurrent architecture: an array containing only the right ventricle and a full tomographic array.

3 Data

In total, 384 3D tomographic volumes (obtained from 24 gated myocardial perfusion SPECT studies, with 16 cardiac phases per study) were analyzed [Larochkin et al., 2025]. The raw data include reconstructed 3D tomographic arrays and the corresponding DICOM files specifying voxel size.

In this work, axes X, Y, and Z follow the index directions of the 3D tomographic array stored in DICOM: X corresponds to the column index, Y to the row index, and Z to the slice number (longitudinal axis).

The dataset was split into training, validation, and test sets with proportions 75 % / 12.5 % / 12.5 %. The annotations were created as follows: for each study and each cardiac phase, the inner and outer surfaces of the RV myocardium were delineated, defining the myocardial wall geometry across all phases [Larochkin et al., 2025].

4 Sequence segmentation model and experiments

For RV myocardial segmentation, a RecurrentUNet3D model built upon a ResUNetSE3D encoder–decoder architecture with skip connections is utilized. The base network is augmented with a convolutional LSTM block at the bottleneck level, which processes features from all cardiac phases of the "representative cardiac cycle" along the temporal axis, explicitly modeling the study's temporal structure. The output is a set of 3D binary RV myocardial masks for each phase. UNet weights are initialized from a pretrained checkpoint, while recurrent layers are trained for the sequence setting.

The main training and architecture settings are summarized in Table 1. The loss function combines binary cross-entropy, Dice loss, and a boundary-aware term.

Input	Dice
RV-only array	0.8119
Full tomographic array	0.7434

Table 2. Segmentation accuracy of the RecurrentUNet3D model evaluated on the test set for two input configurations: an array containing only the right ventricle (RV-only) and the full tomographic volume

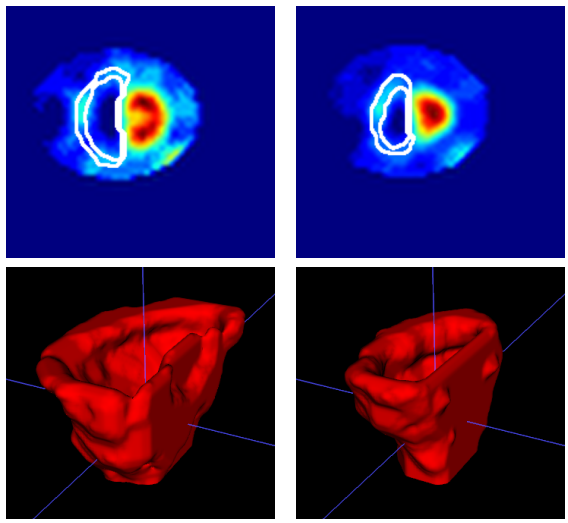

Fig. 1. Examples of manual right-ventricular myocardial delineation for two cardiac phases. Top row: coronal cross-sections with superimposed contours; bottom row: corresponding three-dimensional surface reconstructions of the RV myocardium

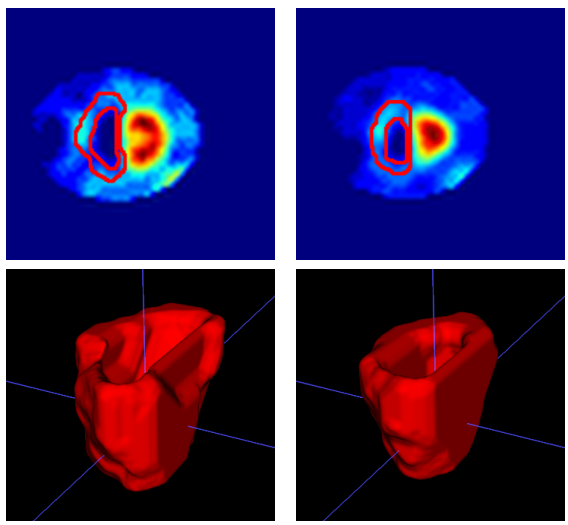

Fig. 2. Segmentation masks predicted by the RecurrentUNet3D model for the same two cardiac phases as in Fig. 1. Top row: coronal cross-sections with predicted contours; bottom row: three-dimensional surface reconstructions

Examples of manual delineations and recurrent-model predictions are shown in Figs. 1 and 2. Segmentation quality (Dice) is summarized in Table 2.

5 Volume curve and derivatives

From the predicted binary masks of the RV myocardium, the endocardial boundary is extracted and a discrete sequence of RV cavity volumes over the "representative cardiac cycle" is formed. The volume at each phase is computed as the number of voxels enclosed by the endocardial boundary multiplied by the physical volume of a voxel obtained from DICOM metadata. The resulting sequence is approximated by a sum of three Fourier harmonics, producing a periodic function $f(t) \approx V(t)$ that describes the RV volume dynamics and enables analytical computation of its first derivative df/dt (see Figs. 3 and 4).

The approximation is defined as

$$f(t) = a_0 + \sum_{n=1}^{3} \left(a_n \cos\left(\frac{2\pi n t}{T}\right) + b_n \sin\left(\frac{2\pi n t}{T}\right) \right), \tag{1}$$

where T is the cardiac-cycle period, N is the number of cardiac phases, and the coefficients are computed from discrete RV cavity volumes V_k ($k = 0, \ldots, N-1$ denotes the phase index):

$$a_0 = \frac{1}{N} \sum_{k=0}^{N-1} V_k, \tag{2}$$

$$a_n = \frac{2}{N} \sum_{k=0}^{N-1} V_k \cos\left(\frac{2\pi n k}{N}\right), \tag{3}$$

$$b_n = \frac{2}{N} \sum_{k=0}^{N-1} V_k \sin\left(\frac{2\pi n k}{N}\right). \tag{4}$$

The first derivative is computed analytically:

$$\frac{df}{dt} = \sum_{n=1}^{3} \frac{2\pi n}{T} \left(-a_n \sin\left(\frac{2\pi n t}{T}\right) + b_n \cos\left(\frac{2\pi n t}{T}\right) \right). \tag{5}$$

From $f(t)$ and its derivative df/dt (shown in Figs. 3 and 4), end-diastolic and end-systolic volumes, as well as additional rate-based indices that characterize RV filling dynamics, are computed.

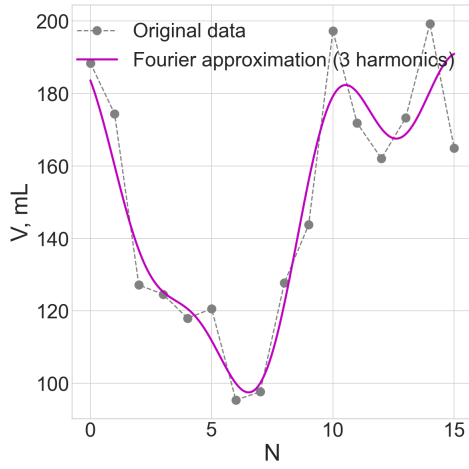

Fig. 3. Discrete right-ventricular cavity volume measured at each cardiac phase (grey markers) and the corresponding smooth approximation obtained as a sum of the first three Fourier harmonics (solid curve)

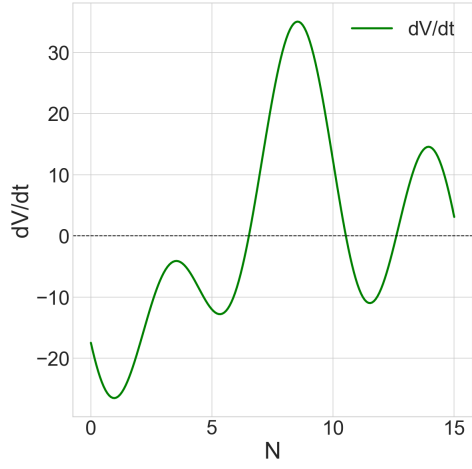

Fig. 4. First derivative df/dt of the Fourier-approximated volume curve, representing the instantaneous rate of right-ventricular cavity volume change across the cardiac cycle

6 Construction of "bull's eye" polar maps

Perfusion polar maps are constructed from the segmentation masks. The "bull's eye" polar map is a standardized 2D representation of 3D myocardial perfusion data [Kotina, 2022].

Given the complex 3D geometry of the right ventricle, an ellipsoidal coordinate system with parameters derived from the RV shape is used for polar map construction.

6.1 Data preprocessing

During preprocessing, the mask is upsampled and smoothed, which reduces noise. The resulting surface representation is illustrated in Fig. 5.

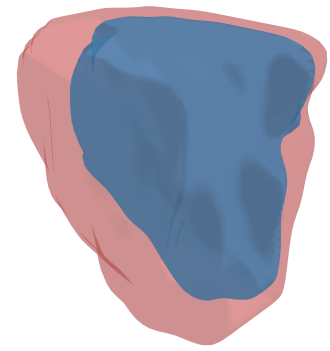

Fig. 5. Three-dimensional polygonal surface models of the right-ventricular epicardium (translucent red) and endocardium (blue), reconstructed from upsampled and smoothed binary segmentation masks via the marching-cubes algorithm

6.2 Geometric parameters and bounding box

From the epicardial surface vertices, an axis-aligned bounding box with limits $x_{\min}$, $x_{\max}$, $y_{\min}$, $y_{\max}$, $z_{\min}$, $z_{\max}$ is computed. The linear dimensions of the right ventricle are computed as

$$L_x = x_{\max} - x_{\min}, \quad L_y = y_{\max} - y_{\min}, \quad L_z = z_{\max} - z_{\min}. \tag{6}$$

The center of the ellipsoidal coordinate system (x_c, y_c, z_c) is selected near the RV base:

$$x_c = x_{\max}, \quad y_c = \frac{y_{\min} + y_{\max}}{2}, \quad z_c = z_{\max}. \tag{7}$$

With this choice, the opposite pole of the ellipsoid ($\varphi = -\pi/2$) corresponds to the RV apex.

6.3 Ellipsoidal coordinate system

The parametric equation of an ellipsoidal surface is

$$\mathbf{S}(\varphi, \theta) = \begin{pmatrix} x_c - a\cos\varphi\cos\theta \\ y_c + b\cos\varphi\sin\theta \\ z_c + c\sin\varphi \end{pmatrix}, \tag{8}$$

where $\varphi \in [-\pi/2, 0]$ is "latitude", $\theta \in [-\pi/2, \pi/2]$ is "longitude", $a = L_x$, $b = L_y/2$, $c = L_z$, and (x_c, y_c, z_c) is the ellipsoid center.

We define the sampling grid as

$$\mathcal{G} = \{(\mathbf{v}_{ij}, \hat{\mathbf{n}}_{ij}) \mid i = 0, \ldots, N_\varphi - 1,\ j = 0, \ldots, N_\theta - 1\}. \tag{9}$$

Here, N_φ and N_θ denote the numbers of sampling nodes along latitude and longitude, respectively. The angular coordinates are sampled on a uniform lattice:

$$\varphi_i = -\frac{\pi}{2} + \frac{i}{N_\varphi - 1} \cdot \frac{\pi}{2}, \quad \theta_j = -\frac{\pi}{2} + \frac{j}{N_\theta - 1} \cdot \pi. \quad (10)$$

Grid vertices are then defined as

$$\mathbf{v}_{ij} = \mathbf{S}(\varphi_i, \theta_j). \quad (11)$$

The resulting grid "wraps" the RV epicardium and approximates its geometry by an ellipsoidal surface. Fig. 6 shows the ellipsoidal coordinate grid aligned with the epicardial polygonal model.

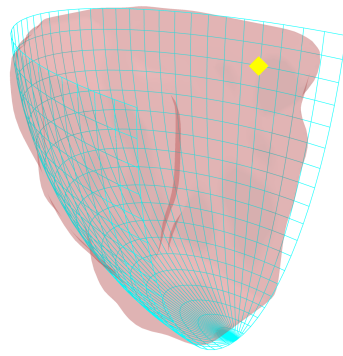

Fig. 6. Ellipsoidal coordinate grid (cyan wireframe) superimposed on the epicardial surface of the right ventricle (translucent pink). The yellow diamond denotes the ellipsoid center, positioned at the apex of the bounding box

6.4 Computing normals and casting rays

To build a polar map, each grid node (i, j) is assigned one perfusion value I_{ij}. For each vertex $\mathbf{v}_{ij}$, intensity is sampled along the local normal. The normal is constructed as follows from the tangential vectors at every sampled node:

$$\mathbf{t}_{\varphi,ij} = \left.\frac{\partial \mathbf{S}}{\partial \varphi}\right|_{(\varphi_i,\theta_j)}, \quad \mathbf{t}_{\theta,ij} = \left.\frac{\partial \mathbf{S}}{\partial \theta}\right|_{(\varphi_i,\theta_j)}, \quad (12)$$

$$\hat{\mathbf{n}}_{ij} = \frac{\mathbf{t}_{\theta,ij} \times \mathbf{t}_{\varphi,ij}}{\|\mathbf{t}_{\theta,ij} \times \mathbf{t}_{\varphi,ij}\|}. \quad (13)$$

Through each vertex $\mathbf{v}_{ij}$, a ray is cast

$$\mathbf{p}(s) = \mathbf{v}_{ij} + s \cdot \hat{\mathbf{n}}_{ij}, \quad s \in \left[-\frac{l}{2}, +\frac{l}{2}\right], \quad (14)$$

where l is the ray length, chosen based on the RV wall thickness. Let $P(\mathbf{p})$ denote the 3D perfusion-intensity volume and $M_{\text{wall}}(\mathbf{p})$ the binary myocardial wall mask. Then, the value projected to node (i, j) is defined as the maximum perfusion intensity along the ray inside the wall:

$$I_{ij} = \max_s \{P(\mathbf{p}(s)) \ : \ M_{\text{wall}}(\mathbf{p}(s)) = 1\}. \quad (15)$$

Figure 7 illustrates the geometric part of the procedure: the ellipsoidal surface $\mathbf{S}(\varphi, \theta)$, the sampling grid nodes $\mathbf{v}_{ij}$, and the corresponding surface normals used for ray casting.

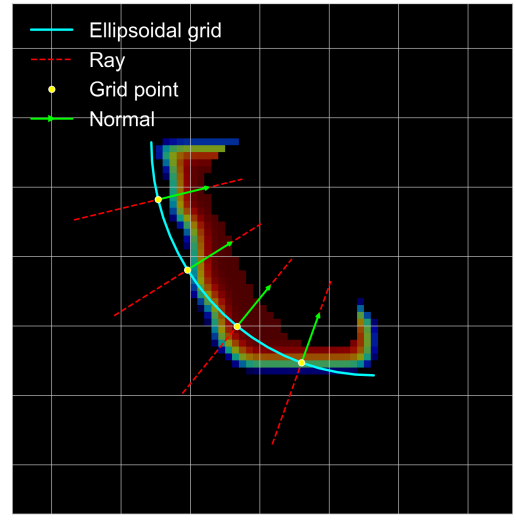

Fig. 7. Ray-casting scheme shown on a 2D cross-section of the myocardial wall. The cyan curve represents the ellipsoidal grid meridian, green arrows indicate surface normals at selected grid points (yellow dots), and red dashed lines show the sampling rays along which maximum perfusion intensity is recorded

6.5 Constructing the planar representation

The coordinate grid of size (N_φ, N_θ) is mapped to a polar chart using the "one node — one cell" rule. The index i (latitude) is mapped to the radial coordinate r, and the index j (longitude) is mapped to the angular coordinate ψ:

$$r = i, \quad \psi = \frac{\pi}{2} + \frac{j}{N_\theta - 1} \cdot \pi. \quad (16)$$

Here, $i = 0$ corresponds to the RV apex (the chart center), while $i = N_\varphi - 1$ corresponds to the base (outer ring). Each polar-map cell stores I_{ij}, i.e., the maximum perfusion intensity along the ray.

For visualization, a color palette widely adopted in nuclear medicine ("PET 20 Step") is used.

Radial and angular partitions of the polar map can be additionally grouped into 9 segments (shown with white boundaries in Fig. 8). An example "bull's eye" polar map constructed using the described method is shown in Fig. 8.

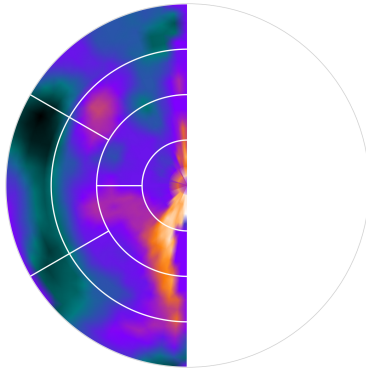

Fig. 8. Right-ventricular myocardial perfusion displayed as a "bull's eye" polar map constructed in the ellipsoidal coordinate system. The colour scale encodes normalized perfusion intensity sampled via ray-casting; white contours delineate standard segmentation regions

Using the same procedure, a "bull's eye" polar map is constructed for each cardiac phase, yielding a temporal sequence $I_{ij}(k)$, $k = 0, \ldots, N-1$, for every grid node (i, j). For node-wise phase analysis, the first-harmonic coefficients are computed as

$$A_{ij} = \frac{2}{N} \sum_{k=0}^{N-1} I_{ij}(k) \cos\left(\frac{2\pi k}{N}\right), \tag{17}$$

$$B_{ij} = \frac{2}{N} \sum_{k=0}^{N-1} I_{ij}(k) \sin\left(\frac{2\pi k}{N}\right). \tag{18}$$

The magnitude and phase maps are then defined by

$$M_{ij} = \sqrt{A_{ij}^2 + B_{ij}^2}, \tag{19}$$

$$\Phi_{ij} = \arctan\left(\frac{B_{ij}}{A_{ij}}\right). \tag{20}$$

Thus, M_{ij} represents the strength of periodic perfusion variation, while Φ_{ij} represents its timing relative to the cardiac cycle. An example is shown in Fig. 9.

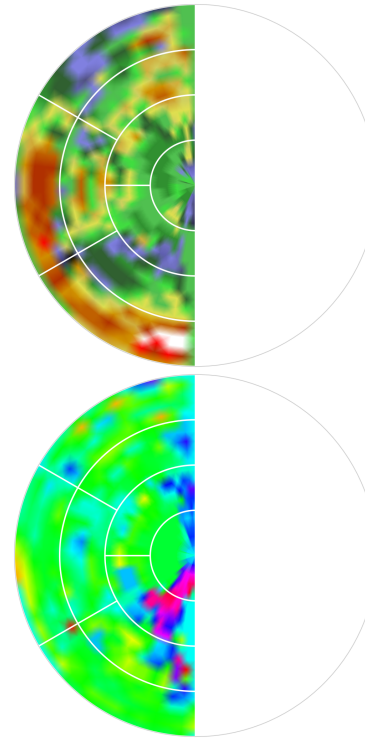

Fig. 9. Magnitude image (top) and phase image (bottom)

Magnitude image reflects the amplitude of periodic perfusion variation, the phase image models the synchrony of myocardial contractions.

7 Conclusion

In experiments, recurrent sequence-based configurations for RV myocardial segmentation in gated SPECT were evaluated for two input representations: an array involving only the right ventricle and a full tomographic array. The corresponding Dice scores were 0.8119 for the array containing only the right ventricle and 0.7434 for the full tomographic array.

Volume curves, functional parameters (end-diastolic and end-systolic volumes, rate-based indices), and "bull's eye" perfusion polar maps together with magnitude and phase maps were obtained from the predicted segmentation masks. These quantitative results constitute clinical data for assessment of right-ventricular perfusion and function.

References

Brunken, R. (2022). Abnormal RV on low-risk SPECT images. Journal of Nuclear Cardiology, 29(4):1915–1918.

Entezarmahdi, S. et al. (2023). Qcard-nm: Developing a semiautomatic segmentation method for quantitative analysis of the right ventricle in non-gated myocardial perfusion spect imaging. EJNMMI Physics, 10:21.

Farag, A. A., Heo, J., Tauxe, L., Bhambhvani, P., Germano, G., Kavanagh, P., et al. (2019). Detection and quantitation of right ventricular reversible perfusion defects by stress spect myocardial perfusion imaging: A proof-of-principle study. Journal of Nuclear Cardiology, 26:266–271.

Jose, A. et al. (2022). Predictive value of incidental right ventricular abnormalities identified on spect for mortality and pulmonary hypertension. Journal of Nuclear Cardiology, 29:1903–1914.

Kotina, E., Ovsyannikov, D., Ostroumov, E., et al. (2014). Indis-karfi: Program for processing functional cardiac studies. Registered software certificate No. 2014662434.

Kotina, E. D. (2022). Mathematical and computer modeling in nuclear medicine [Matematicheskoe i komp'yuternoe modelirovanie v yadernoy meditsine]. VVM, Saint Petersburg. In Russ.

Larochkin, P., Kotina, E., Girdyuk, D., and Ostroumov, E. (2025). Deep learning methods for right ventricle segmentation in radionuclide imaging. Cybernetics and Physics, 14(1):62–66.

Mannting, F., Zabrodina, Y. V., and Dass, C. (1999). Significance of increased right ventricular uptake on 99mtc-sestamibi spect in patients with coronary artery disease. Journal of Nuclear Medicine, 40:889–894.

Meyer, P., Filippatos, G. S., Ahmed, M. I., Iskandrian, A. E., Bittner, V., Perry, G. J., et al. (2010). Effects of right ventricular ejection fraction on outcomes in chronic systolic heart failure. Circulation, 121:252–258.

Ostroumov, E. N., Kotina, E. D., Senchenko, O. R., and Mironkov, A. B. (2010). Radionuclide methods in cardiological practice. Serdtse: Zhurnal dlya praktikuyushchikh vrachei [Heart: Journal for Practitioners], 9(3):190–195. In Russ.

Ploskikh, V. and Kotina, E. (2018). Quantitative analysis of gated myocardial perfusion spect. Cybernetics and Physics, 7:220–227.

Ploskikh, V. and Kotina, E. (2021). Challenges of gated myocardial perfusion spect processing. Cybernetics and Physics, 10(3):171–177.

Rich, J. and Ward, R. (2010). Right-ventricular function by nuclear cardiology. Current Opinion in Cardiology, 25(5):445–450.

Ryzhkova, D. (2016). Myocardial perfusion scintigraphy. Cardiology: News, Opinions, Training, 4:76–86.

Schmidt, I., Kotina, E., and Buev, P. (2023). Deep learning muscle segmentation model for ct images in dicom format. Cybernetics and Physics, 12(3):201–206.